Article

An Experimental Investigation of the Effect of Interfacial Waves on the Evolution of Sliding Zones in a Liquefied Seabed

Xiaolei Liu [1,2], Xingyu Li [1], Hong Zhang [3,*], Yueying Wang [1], Qiang Zhang [4], Haoqiang Wei [3] and Xingsen Guo [1,3,5]

1. Shandong Provincial Key Laboratory of Marine Environment and Geological Engineering, Ocean University of China, Qingdao 266100, China; xiaolei@ouc.edu.cn (X.L.); 21201031155@stu.ouc.edu.cn (X.L.); wyy98@stu.ouc.edu.cn (Y.W.); xingsen.guo@ucl.ac.uk (X.G.)
2. Laboratory for Marine Geology, Qingdao Marine Science and Technology Center, Qingdao 266237, China
3. College of Engineering, Ocean University of China, Qingdao 266404, China; 21230911130@stu.ouc.edu.cn
4. Shandong Provincial Bureau of Geology & Mineral Resources, Jinan 250013, China; qddkzq@163.com
5. Department of Civil, Environmental, and Geomatic Engineering, University College London, London WC1E 6BT, UK
* Correspondence: zhanghong9645@ouc.edu.cn

Abstract: The sliding process of liquefied submarine landslides is generally regarded as being induced by the coupling of excess pore pressure accumulation and shear stress under surface wave action. However, the significant role of interfacial waves formed over the seabed surface upon liquefaction has been largely ignored. The characteristics of interfacial waves and their effect on the development of a seabed sliding zone are poorly understood. Wave flume experiments were conducted to observe the occurrence and evolution of the interfacial wave and sliding zone, combined with image analysis to extract interfacial wave parameters. The results show that the shear action of interfacial waves can cause progressive liquefaction sliding of the seabed and the formation of a sliding zone. The specific location and thickness of the sliding zone are always dynamically changing during the liquefaction development process and are consistent with the liquefaction depth. The wave height of liquefaction interfacial waves increases with liquefaction depth, and the maximum ratio of interfacial wave height to surface wave height can reach 0.175, corresponding to a maximum longitudinal width ratio of the sliding zone of 0.25. The continuously developing interfacial waves transfer the energy of surface waves to deeper areas, expanding the limit depth of sliding zone evolution. This study can provide theoretical guidance for the prevention and control of seabed instability and sliding disasters under extreme storm conditions.

Keywords: liquefaction; interfacial wave; sliding zone; submarine landslides; seabed stability

1. Introduction

Seabed stability poses a significant importance to the safety of marine engineering facilities such as offshore drilling platforms and submarine pipelines [1]. However, multiple external factors (waves, earthquakes, hydrate decomposition, etc.) cause seabed instability such as liquefaction, scour, and shear slide to occur frequently [2–4]. The sliding zone, generated through folding and shearing on the sliding surface during seafloor instability, is an essential part of landslides [5]. The physical and mechanical characteristics of sediments in sliding zones, including sediment type, particle composition, and microscopic structure, are closely related to the evolutionary development and landslide stability evaluation [6,7]. Therefore, the study of the sliding zone holds immense importance in identifying the deformation and failure mechanism of submarine landslides, mitigating marine geological disasters, and ensuring the sustainable development of the marine economy.

Wave-induced seabed instability is the most common sliding geohazard in delta and shallow water regions [8,9]. A multitude of systematic studies of the seafloor instabilities

in this region have been conducted [10–12]. Taking the Yellow River Subaqueous Delta as an illustration, earlier research frequently attributed seafloor instability in the area to wave-induced shear failure [10]. The shear stress exerted by waves on the seabed is proved to be a key factor for triggering submarine landslides in the Yellow River Subaqueous Delta through laboratory tests and in situ observation [1,10]. Subsequently, scholars gradually recognized that liquefaction induced by waves is also an important factor leading to the deformation and sliding of the seabed [13,14]. Model experiments about the liquefaction of saturated non-viscous or silty sediments found that the liquefaction is related to the gradual development of pore pressure [15–19]. The reason for wave-induced seabed liquefaction is identified to be the redistribution of excess pore water pressure caused by damping and phase lag [17,18]. The threshold of pore water pressure for the liquefaction of soft sediment through laboratory flume experiments was established [19]. The pore water pressure in seabed sediments showed different degrees of lag accumulation characteristics at different depths during wave action through tidal flat tests, and the strength of sediments was not completely lost when the excess pore water pressure exceeded the overlying pressure through a wave flume test [20,21]. It was found that the existing methods may underestimate the potential for seabed liquefaction and that the nonlinear effect of waves on promoting seabed liquefaction is more significant in progressive waves than in standing waves. The coupling effect between pore water pressure development and seabed stress evolution was investigated and used to improve the existing decoupling methods [17,18]. A model for evaluating the seabed instability (e.g., liquefaction, erosion, seepage, and shear sliding) and geological hazards (e.g., shallow surface landslides, pockmarks, mudflows, disturbance layers, and hard shells) of sandy seabed caused by storm surges was established based on the coupling effect in the Yellow River Subaqueous Delta [22]. To sum up, previous studies generally analyzed seafloor sliding from the perspective of shear caused by surface waves and liquefaction, with little attention paid to the interfacial waves formed on the seafloor by liquefied sediment.

Wave-induced liquefied sediment is assumed to be a kind of fluid with mass density [23,24]. The two-layer fluid theory was introduced first to consider the liquefied sediment as a fluid based on the theory proposed by Lamb (1932) [25]. A two-layer fluid model for the liquefaction problem was established when analyzing the propagation law of the sand liquefaction zone under the action of waves and currents [26]. The model was modified by considering parameters such as viscosity [26–31]. The movement trajectory of liquefied sediment particles under shallow-water small-amplitude waves was observed to be elliptical based on the new two-layer fluid model and wave flume experiments, and analytical solutions were given for the movement and displacement of sandy liquefied sediment particles under wave action using small-amplitude wave theory and fluid wave depth reference surface setting methods [27–29]. However, the change law of the interfacial wave and the internal shear stress caused by it, as well as its influence on the sliding zone during the development of seafloor liquefaction, are still unclear. In this paper, the wave flume experiment simulated the liquefied sliding phenomenon of the seabed was conducted to obtain the evolution characteristics of the sliding zone, and then the parameters of the interfacial wave were obtained through the image processing of liquefied seabed video images through the Matlab program platform. Finally, the influence of the interfacial wave on the evolution of the sliding zone was analyzed according to the changes in the interfacial wave during the liquefied sliding process. The results of this study could provide theoretical support for disaster prevention and control under extreme storm conditions.

2. Materials and Methods

2.1. Wave Flume Experiment

The experiment was carried out within a wave flume with dimensions of 5 m in length, 0.4 m in width, and 1 m in depth. Figure 1 illustrates the layout of the experimental flume. A piston-type wave generator was used to produce progressive surface waves. At the far end of the flume, a wedge-shaped wave absorber was installed to dissipate the surface

wave energy. In the middle of the flume, an iron bed measuring 1.2 m long and 0.3 m deep was placed to simulate the seabed. To ensure a smooth transition in the overall water depth, a false-bottom platform was set up between the seabed and the wave generator. Pore pressure transducers were embedded in the sediment at depths of 5 cm and 15 cm below the seabed surface to monitor changes in pore pressure under dynamic wave loading, which is critical for analyzing seabed stability. The transducers used in this study were model 86 from Joint Sensor Instruments, piezoresistive sensors developed by the Nanjing Hydraulic Research Institute, China, with a diameter of 80 mm and a height of 20 mm. A turbidity meter was set up on the seabed surface to measure the change in seawater turbidity during the liquefaction process. The turbidity was measured in NTU (Nephelometric Turbidity Units) using RBR T. D designed by the Canada RBR Company. Equipped with conductivity sensors, temperature sensors, and pressure sensors, the instrument can be used to correct turbidity data. Considering the linear correlation between the undrained shear strength and the penetration resistance, the shear strength of the sediment was represented by the penetration resistance measured by one portable cone penetration test probe with a diameter of approximately 15 mm.
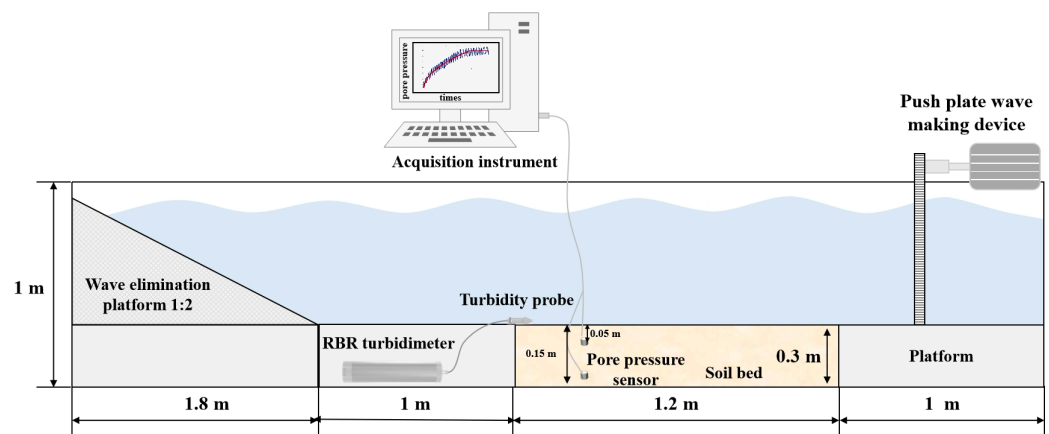

Figure 1. Sketch of the wave flume.

The sediment samples collected from the Yellow River estuary abandoned lobe were used to prepare the seabed in the experiment. The sediment samples were dried, ground, and sieved to remove impurities like shells before the experiment. Then, the weighed sediment samples were mixed with water in a blender with a desired water content of 33%, which is the average natural water content of the Yellow River Delta sediment. The mixture was stirred into a homogeneous slurry and was then slowly poured along the flume wall into the sediment tank up to about 30 cm thick. Water, 55 cm in depth, was then gradually added into the wave flume after the seabed was laid. The physical parameters of the initial seabed, such as bulk density, water content, liquid limit, and particle size composition, were measured before the experiment (Table 1). The seabed sediments were left to consolidate under gravity for 48 h before the flume experiment started. A wave loading of approximately 12 cm high was imposed using the wave generator mounted at the end of the flume to let the seabed reach the liquefaction state. The wave loading was stopped when the seabed reached different liquefaction depths (11 cm, 14 cm, 17 cm, and 20 cm; retracted to 16 cm was selected in this experiment), and the penetration resistance was tested. High-concentration fluid was extracted at the corresponding stages and subjected to density measurement in a 100 mL density bottle. In the liquefaction retraction phase, the columnar samples of a stable seabed, sliding seabed, and re-consolidation seabed were collected to investigate the physical and mechanical characteristics of the sediment. The difference between sliding zone sediment and sediment in the upper and lower regions of the sliding zone was compared. To avoid taking samples too close to the edge wall and to ensure that the liquefaction depth of the seabed in the center of the sediment tank was close

to the bottom of the tank, the sampling position was selected at one-third of the distance from the left side of the sediment tank.

Table 1. Basic physical properties of the sediment sample used in the experiment.

Density (kg/m³)	Water Content (%)	Liquid Limit	Plastic Index	Grain Composition		
				Clay (%)	Silt (%)	Sand (%)
1870	33	27	11	15	54.2	30.8

The liquefaction criterion proposed by Zen et al. (1998) was adopted in this study [32], which states that when the excess pore pressure P_e is greater than or equal to the initial mean normal effective stress σ_0' of the overlying sediment, liquefaction occurs at that location. The expression is as follows:

$$\sigma_0' \leq P_e \tag{1}$$

$$\sigma_0' = \gamma' z \frac{1 + 2K_0}{3} \tag{2}$$

$$P_e = P - P_b \tag{3}$$

where γ' is the effective unit weight of the sediment, and the value of 790 kg/m³ was adopted; z is the thickness of the overlaying sediments; K_0 is lateral pressure modulus given by $K_0 = \sigma_h'/\sigma_v'$, and was taken as 0.5 as the average value of the tested sediment; P is the pore water pressure induced by a wave; and P_b is the wave pressure at the seabed.

2.2. Measurement of the Interfacial Waves

The interfacial waves that appeared in the experiment were recorded with a mobile terminal (Canon R5) with a high-definition video recording function at a speed of 30 fps. The image processing technology was used to realize the quantitative measurement of the interfacial wave under the experimental conditions. Based on the Matlab program platform, morphological processing methods were used to process the test process recorded by video, and the wave height, period, amplitude, and other interfacial wave experimental data were obtained. The recorded video was converted into a still image with a pixel of 1980 × 1080. The image was extracted at a speed of 3 Hz, and binary conversion, noise reduction, filtering, edge detection, and other operations were performed to obtain the fluctuation boundary of each frame image. According to the scale set in the sediment tank, coordinate transformation was performed to obtain the fluctuation parameters in the data acquisition area of the image. According to the frame rate of the video, the corresponding relationship between the frame position and time was established, and the time series of a fixed position fluctuation in the image acquisition area was obtained.

The liquefied sediment in this study is viewed as a kind of fluid with mass density, and interfacial wave research was conducted based on the two-layer fluid model (Figure 2). The wave-induced shear stress on the seabed is mainly caused by changes in the direction of internal pressure in the seabed [19]. According to the linear wave theory of progressive waves, the pressure gradient along the direction of wave propagation on the seabed surface is given by the following equation:

$$\frac{\partial p}{\partial x} = \frac{\rho g a k}{cosh k d} \cos(kx - \omega t) \tag{4}$$

where ρ is fluid density; g is taken as 9.81 m/s²; a is amplitude; k is the wave number equal to $2\pi/L$; d represents fluid depth, which consists of water depth d_w and the liquefied seabed depth d_{ls}; and ω represents wave frequency. The maximum shear stress generated by interfacial waves can be calculated by the following equation [33]:

$$\tau_{max} = \hat{p} k z e^{-kz} \tag{5}$$

$$\hat{p} = \frac{\rho g a}{\cosh kd}\left(\frac{F'}{F' - \tanh kd}\right) \tag{6}$$

$$F' = \frac{Gk^2}{\rho \omega^2 (1 - \varnothing)} \tag{7}$$

where $\hat{p}$ is the amplitude of the pressure at the sediment–water interface; z is the depth, which is positive downward at the water–sediment interface; G is the shear modulus; and $\varnothing$ is Poisson's ratio.
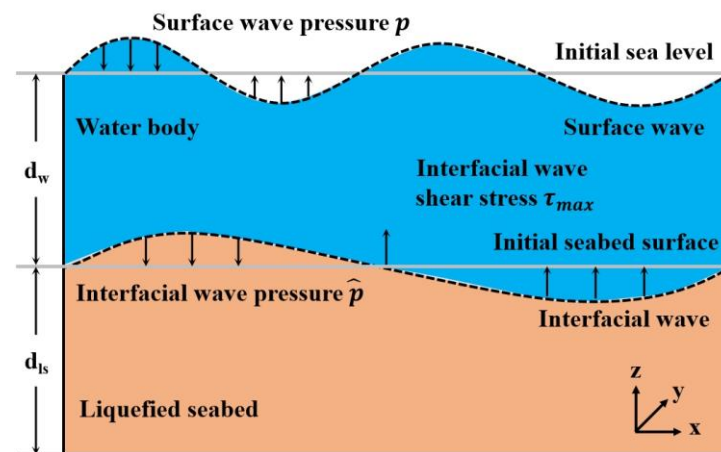

**Figure 2.** Configuration of the two-layer fluid system (after Sassa et al., 2001 [26]).

3. Results and Analysis

### 3.1. Development of the Sliding Zone during the Wave Flume Experiment

Figure 3 shows the alteration in the pore pressure at diverse depths and the turbidity of the seabed surface throughout the entire experiment process. With the advancement of the 12 cm high wave action, the pore pressures at the depths of 5 cm and 15 cm rose steeply at the beginning and declined slightly afterward. The excess pore water pressure peaked at 0.75 kPa and 1.4 kPa approximately at 6 min and then decreased gradually. According to Equation (2), the estimated initial mean normal effective stress of the sediment was approximately 0.26 kPa and 0.79 kPa for overlaying sediment thicknesses of 5 cm and 15 cm, respectively. Figure 3 reveals that the excess pore pressure at depths of 5 cm and 15 cm were both larger than the initial mean normal effective stress of the sediment, indicating that the sediment layer had undergone liquefaction. The turbidity data demonstrate a corresponding tendency. The turbidity rose rapidly along with the sudden increase in pore pressure, reaching a maximum of 100 NTU at 32 min, followed by a gradual decrease.

The array of features can be observed in the flume experiments (Figure 4). When excess pore pressure initiated its accumulation, minoroscillatory mud ripples emerged on the seabed surface (Figure 4A). Under the continued application of wave loading, the mud ripples gradually extended across the seabed surface, resulting in the liquefaction of the seabed (Figure 4B). Figure 4C shows the evolution of the liquefaction boundary expanding with time. The maximum liquefaction depth in this experiment is 0.2 m (Figure 4D). The sliding zone formed when the liquefied sediment slid left and right along the concave interface (Figure 4C,D). The liquefaction bottom boundary began to rise, and the stratum that passed through was re-stratified (Figure 4E). The process of liquefaction stopped, and the seabed sank by approximately 5 cm (Figure 4F).
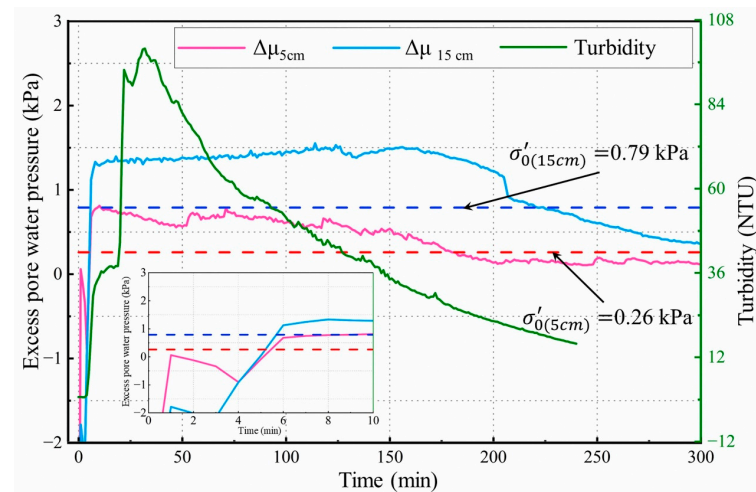
Figure 3. Development of pore pressure at different depths of seabed and turbidity at the seabed surface.
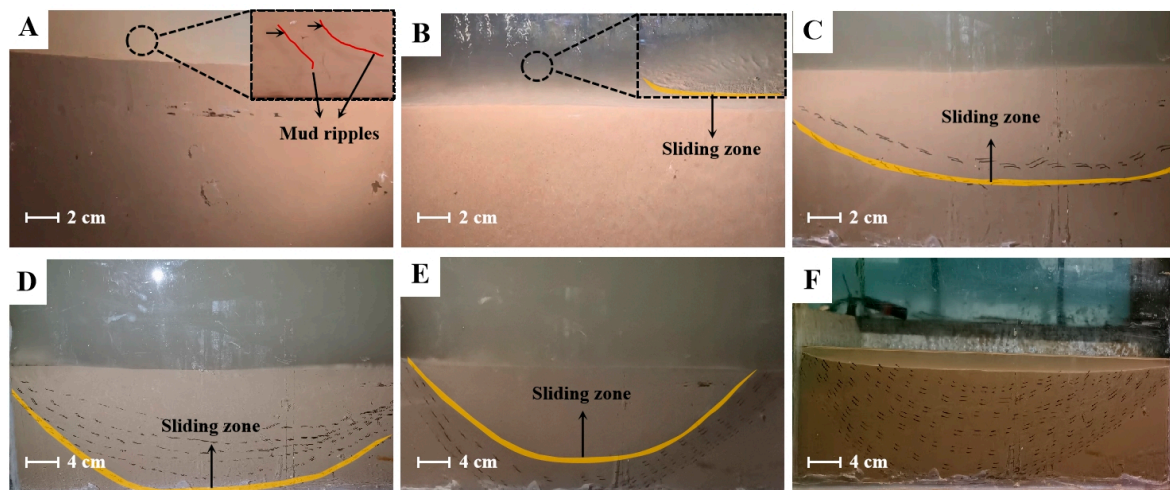
Figure 4. Records of phenomena at various stages of the flume test. (**A**) The mud ripples appeared at the initial stage of the flume test. (**B**) The seabed began to liquefy, and the sliding zone came to being. (**C**) The sliding zone expand downward as the evolution of the liquefaction boundary expanded with time. (**D**) The largest sliding zone formed when the maximum liquefaction depth was reached. (**E**) The sliding zone moved upward when the liquefaction depth decreased with time. (**F**) Both the liquefaction and sliding process were over.

Figure 5 presents the vertical profile of the sliding zone along with the grain size distribution and the penetration strength of the sediment. Specific locations of the sliding seabed, sliding zone, reconsolidated sediment layer, and the original sediment layer are also marked. The trend in the penetration strength of the sediment shows an initial increase followed by a decrease with depth. The CT image and grain size distribution both indicate that the sediment was re-stratified. The stable sediment layer at the bottom, which did not slide, consists of uniform sandy silt particles. The sliding seabed at the top is dominated by clayey sediment particles of relatively uniform size. The reconsolidated stable layer above the non-sliding layer has relatively fewer clay particles compared to the sliding zone, and between these two layers is the sliding zone where clay content gradually decreases with depth. The penetration strength of the original sediment layer is less than 3 N, and it is close to 0 N. The sliding zone is a transition zone with a sudden increase in strength from around 3 N to 8.3 N. The strength value of the sediment at the reconsolidated sediment

layer increases to 10 N, whereas the strength of the original soil layer is approximately 3.5 N.
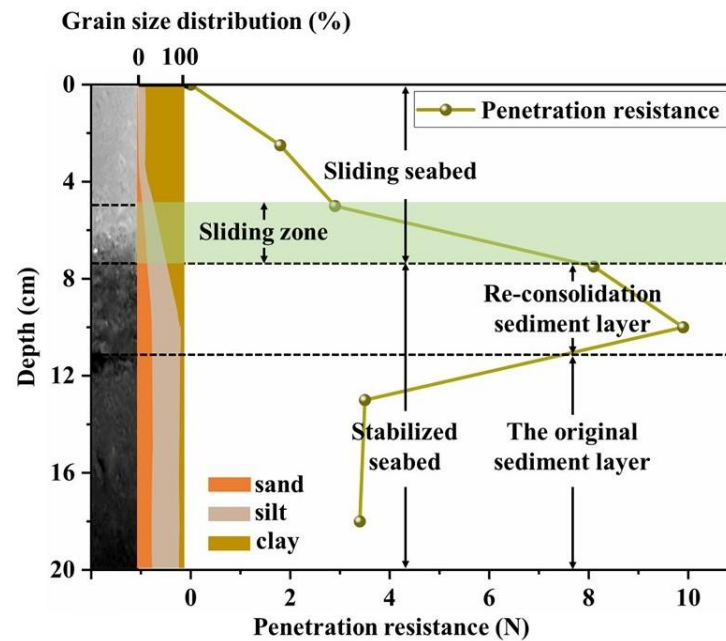
Figure 5. Sediment particle composition and penetration resistance in the upper and lower regions of the sliding zone.

### 3.2. Characteristics of the Liquified Interfacial Wave

The typical wave time series of the liquefied interfacial waves were extracted when the liquefaction depth was 11 cm, 14 cm, 17 cm, and 20 cm and during the onset of liquefaction contraction through the image method (as shown in Figure 6). The wave parameters for each stage are recorded in Table 2.

Table 2. Surface and interfacial wave parameters.

	Wave Height/h (m)	Wavelength/λ (m)	Period/T (s)	Density/ρ (kg/m³)	Wave Number/k	Fluid Depth/d (m)	Shear Stress/τ (Pa)
Surface wave	0.120	2.28	1.27	1025	2.76	0.55	697
Stage 1	0.004	1.32	1.33	2104	4.76	0.11	172
Stage 2	0.005	1.48	1.33	2093	4.25	0.14	184
Stage 3	0.007	1.61	1.33	2091	3.90	0.17	228
Stage 4	0.020	1.72	1.33	2081	3.65	0.20	578
Stage 5	0.010	1.69	1.33	2067	3.72	0.19	299

In this experiment, the position of the sliding zone was located at the interface of the liquefied seabed and initial seabed, which corresponded to the liquefaction depth. When the liquefaction depth was 11 cm, the interfacial wave was relatively unstable with a small amplitude of around 4 mm (Figure 6A). As the sliding zone continued to move downward, the waveform became more stable. When the liquefaction depth was 14 cm, the amplitude of the interface wave increased slightly to about 5 mm (Figure 6B). When the liquefaction depth reached 17 cm, the amplitude of the interfacial wave continued to increase slowly, reaching approximately 7 mm (Figure 6C). When the liquefaction depth reached the peak value of 20 cm, the amplitude of the interface wave increased rapidly to around 20 mm (Figure 6D). After the liquefaction started to retract, the amplitude of the interfacial wave also decreased. Under the surface wave with an amplitude of 12 cm and a period of 1.27 s, the period of the interfacial wave was generally around 1.33 s throughout the evolution of the sliding zone, which was slightly higher than the surface wave and

generally consistent it (Figure 6E). Overall, the liquefaction interfacial wave presented a relatively stable waveform in the time sequence. The frequency of the interfacial wave was nearly consistent with the surface wave, slightly lower than it, while the wavelength and amplitude were much smaller than the surface wave. The interfacial wave was in essence a subharmonic resonance caused by the surface wave resonating on the seabed.
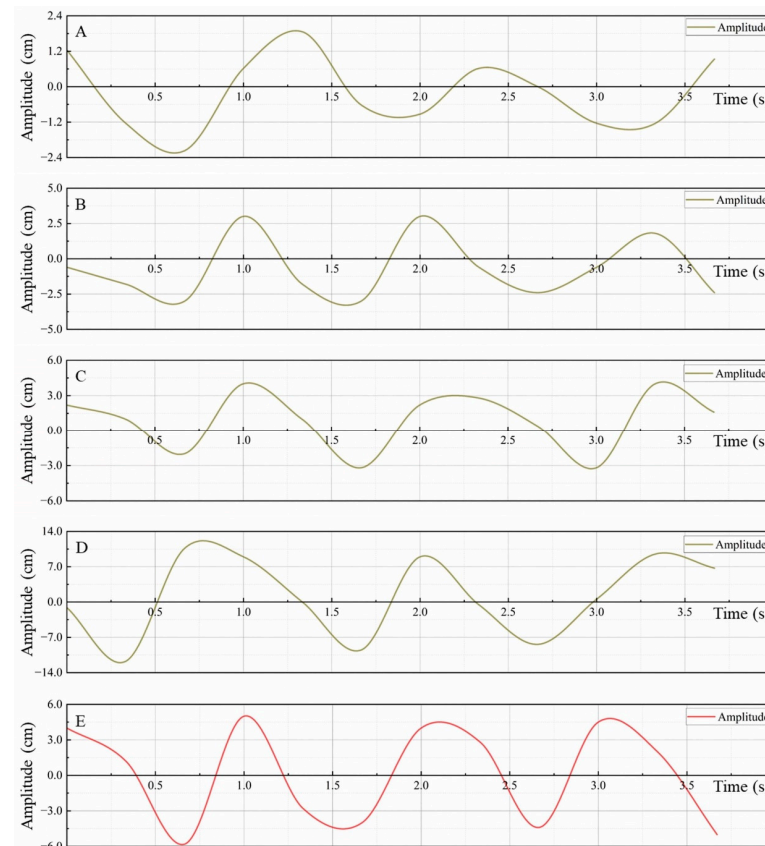
Figure 6. Time series of interfacial waves at a fixed position. Time series of an interfacial wave when the depth of liquefaction is (**A**) 11 cm, (**B**) 14 cm, (**C**) 17 cm, and (**D**) 20 cm. (**E**) Time series of an interfacial wave when liquefaction began to retract.

4. Discussion

4.1. The Evolution of Sliding Zone

The sliding zone is generated because of the liquefaction-induced sliding of sediment, and its thickness progressively augments during the downward progression of the sliding zone. As shown in Figure 5, the thickness of the sliding zone can increase to about 2 cm under the experimental conditions. Figure 7A illustrates the evolution process of the interfacial wave and the sliding zone. The wave height of the interfacial wave increased first and then decreased, and the sliding zone also has a corresponding evolution trend. A series of features observed in the flume experiments can be incorporated into a new model of interfacial wave-induced evolution of the sliding zone. As mentioned above, liquefaction sliding is caused by the coupling effect of wave-induced liquefaction and shearing. This model integrates the process of interfacial wave-induced sediment sliding—including the evolution of the sliding zone and the development of interfacial waves. Under the wave action, mud ripples first appear on the seabed surface, resulting in local interfacial waves. As the liquefied sediment begins to fluctuate, sliding zones initially form beneath it. The shear stress on the seabed sediment is directly applied by the surface wave in this stage. A continuous fluctuating stable interfacial wave with a period of about 1.33 s was generated due to the sliding of the liquefied sediment after the mud ripples spread over the entire surface (stage 1 in Figure 7A). The local sliding zone evolved into a continuous intact

sliding zone due to the relative sliding between the fluctuating liquefied sediment and the stable seabed. The bottom boundary of liquefied sediment continued to decline under the action of waves and reached a maximum depth (0.2 m), and the thickness of the sliding zone increased gradually from 0 to the highest level (about 2 cm) (stage 2 in Figure 7A). The depth and width of the sliding zone began to retract after reaching the maximum depth (stage 3 in Figure 7A). In a practical seabed, due to the non-uniform distribution of interfacial waves, the liquefied sediment will slide in the form of flow slides in the evolution process under the action of many factors such as slope and waves. The sliding zone undergoes secondary evolution in the process (stage 4 in Figure 7A).
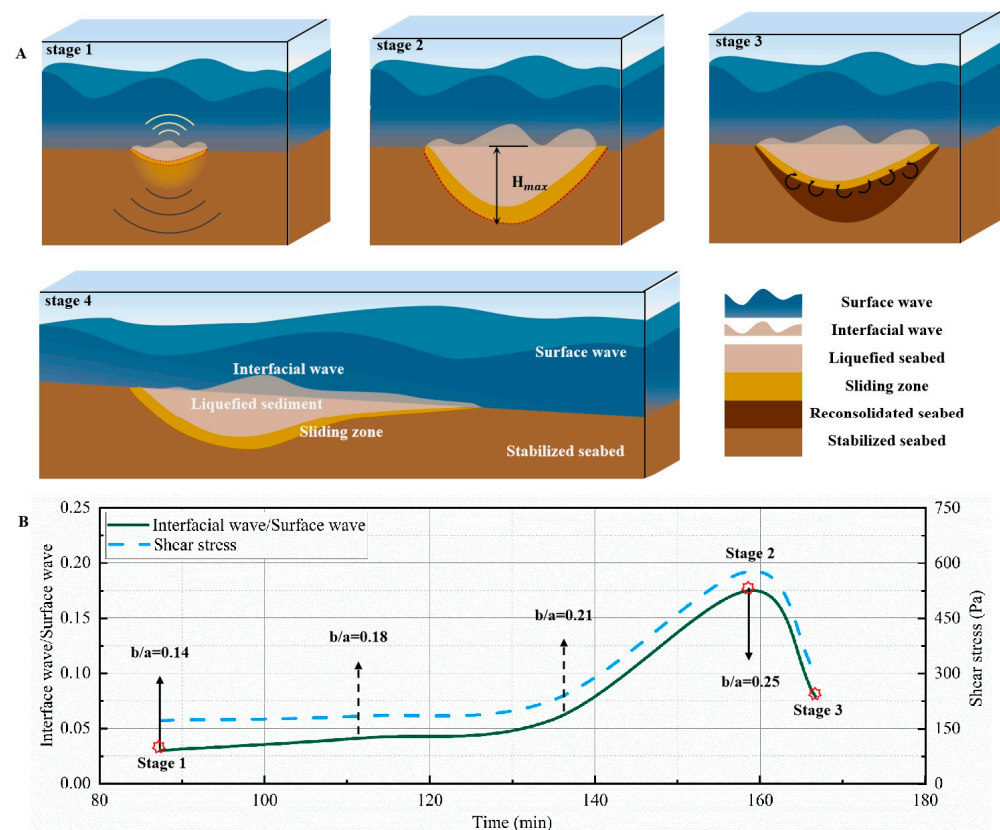
Figure 7. (**A**) Schematic of the evolution of the sliding zone induced by interfacial waves during the development of an interfacial wave. In stage 1, the interfacial wave and the sliding zone were generated due to the sliding of the liquefied sediment. The bottom boundary of liquefied sediment reached a maximum depth, and the thickness of the sliding zone increased gradually from 0 to the highest level in stage 2. Then the depth and width of the sliding zone began to retract in stage 3. The sliding zone undergoes secondary evolution under the action of many factors such as slope and waves. (**B**) Curves of the ratio of the interfacial wave height to the surface wave height and the corresponding shear stress.

4.2. The Effect of Interfacial Waves

The interactions between surface waves and interfacial waves have been addressed by many studies [27–29]. The energy of surface waves can only affect shallow sediment layers due to the dissipation of wave energy in the seabed [34–37]. The action of surface wave can only cause liquefaction in a certain range of the seabed surface when the interfacial wave can continuously shear the underlying sediment layers. According to Figure 3, the sustained action of interfacial waves leads to a slow dissipation of pore pressure [38]. During the period in which interfacial waves exist, high pore pressure values can still be maintained, leading to the downward movement of the sliding zone along with the

continuous development of the range of liquefaction slide. Therefore, interfacial waves, to some extent, delayed the attenuation of energy transfer to deeper sediment layers [39,40].

According to Equations (4) and (5), the maximum shear stress generated by surface waves and liquefaction interfacial waves was estimated (Table 2). The shear stress caused by the surface waves within the sediment was about 697 Pa, while the shear stress induced by interfacial waves was similar in magnitude to that induced by surface waves and increased with wave height within the measurement range, ranging from a minimum of 172 Pa to a maximum of 578 Pa. Figure 7B shows the variation in the interfacial wave height and corresponding shear stress with the evolution of the sliding zone. As the sliding zone evolved deeper into the seabed, the wave height gradually increased and then decreased during the retraction of liquefaction. Previous simulation experiments based on traditional two-layer fluid models suggested that the propagation of interfacial waves would be limited when the phase angle between the surface and interface increased when liquefaction reached deeper [41]. This study suggests that the growth of interfacial waves is also influenced by sediment strength and other properties. During the initial development of the sliding zone, the growth of interfacial wave height was slow, as the original seabed strength was low, and the penetration resistance was only about 3 N. The interfacial wave continuously sheared the seabed, resulting in a continued increase in the depth of the liquefaction slide and an increase in the interfacial wave height. The rate of increase in the interfacial wave height accelerated when the depth of the sliding zone reached 17 mm until the sliding zone evolved to its deepest (20 mm), and then the interfacial wave height decreased. The stratum was re-stratified due to the differentiation and re-deposition of sediment particles [40–43]. The sediment strength is significantly enhanced, and a high-strength reconsolidated sediment gradually forms, which is not easily broken by the shear stress induced by the interfacial wave. The growth of the interfacial wave was limited by the reconsolidated sediment.

The depth b of the sliding zone and width a of the trench are defined as the longitudinal width ratio of the sliding zone, and the interfacial wave height is non-dimensionalized through the utilization of the ratio of the interfacial wave height to the surface wave height. As presented in Figure 7B, within the first 130 min before the onset of liquefaction, the ratio of the interfacial wave height to the surface wave height was less than 0.05, signifying the initial liquefaction stage. The liquefied area was small, and during this stage, the interfacial wave gradually stabilized, and it also constituted a fast-evolving stage of the sliding zone. As liquefaction continued to evolve, the particle coarsening effect continued, and the influence of interfacial wave height growth on the sliding zone evolution weakened until the maximum value of the ratio of interface wave height to surface wave height reached 0.175. Subsequently, a high-strength reconsolidated soil was produced, and the shear force caused by the interfacial wave was insufficient to break the soil, resulting in the contraction of the sliding zone.

Under the conditions of this experiment, the maximum ratio of interfacial wave height to surface wave height was found to be 0.175, corresponding to a maximum sliding zone aspect ratio of 0.25. In actual observation surveys, sliding zones on the seafloor are difficult to identify. Therefore, the maximum ratio of interface wave height to surface wave height determined through experiments can be used in conjunction with geophysical data to indirectly determine the width, depth, and extent of sliding zones in the survey area.

5. Conclusions

This paper studied the influence of liquefaction–induced interface waves on sliding zones through a series of flume experiments. The conclusions are as follows:

(1) Liquefaction-induced interfacial waves are formed on the seabed surface due to wave-induced liquefaction, with a slightly smaller period than surface waves. The size of the interfacial waves is mainly controlled by the amplitude.

(2) The growth of interfacial waves is significantly affected by the strength of the seabed. In low-strength original seabed, interfacial waves can continue to grow until they are suppressed and recede after the formation of high-strength reconsolidated sediment.

(3) The development of sliding zones under the influence of interfacial waves shows a pattern from non-existence to existence, and the influence of interfacial wave height on the evolution rate of sliding zones gradually decreases with the development of liquefaction.

(4) In a homogeneous silty seabed, the maximum ratio of the interfacial wave height to surface wave height is 0.175, corresponding to the maximum longitudinal width ratio of sliding zones of 0.25. Combined with geophysical data in the study area, the depth and range of sliding zones can be determined.

Author Contributions: Conceptualization, H.Z. and X.L. (Xiaolei Liu); methodology, X.L. (Xingyu Li) and Y.W.; formal analysis, X.L. (Xingyu Li), Y.W. and H.W.; investigation, X.L. (Xingyu Li), Y.W., Q.Z. and H.Z.; data curation, X.L. (Xingyu Li) and X.G.; writing—original draft preparation, X.L., X.L. (Xingyu Li) and H.Z.; writing—review and editing, H.Z., X.G. and X.L. (Xiaolei Liu); visualization, Y.W. and H.W.; supervision, X.L. (Xiaolei Liu) and X.G.; project administration, X.L. (Xiaolei Liu) and H.Z. All authors have read and agreed to the published version of the manuscript.

Institutional Review Board Statement: Not applicable.

Informed Consent Statement: Not applicable.

Data Availability Statement: All data from this paper are available upon request. Please contact Hong Zhang at zhanghong9645@ouc.edu.cn.

Conflicts of Interest: The authors declare no conflicts of interest.

References

1. Guo, X.S.; Liu, X.L.; Zheng, T.Y.; Zhang, H.; Lu, Y.; Li, T.T. A mass transfer-based LES modelling methodology for analyzing the movement of submarine sediment flows with extensive shear behavior. *Coast. Eng.* **2024**, *191*, 104531. [CrossRef]
2. Fan, N.; Jiang, J.X.; Nian, T.K.; Dong, Y.K.; Guo, L.; Fu, C.W.; Tian, Z.C.; Guo, X.S. Impact action of submarine slides on pipelines: A review of the state-of-the-art since 2008. *Ocean Eng.* **2023**, *286*, 115532. [CrossRef]
3. Liu, X.L.; Wang, Y.Y.; Zhang, H.; Guo, X.S. Susceptibility of typical marine geological disasters: An overview. *Geoenviron. Disasters* **2023**, *10*, 10. [CrossRef]
4. Jamil, M.; Siddiqui, N.A.; Umar, M.; Usman, M.; Ahmed, N.; Rahman, A.H.; Zaidi, F.K. Aseismic and seismic impact on development of soft-sediment deformation structures in deep-marine sand-shaly Crocker fan in Sabah, NW Borneo. *J. King Saud Univ. Sci.* **2021**, *33*, 101522. [CrossRef]
5. Chen, Q.; Cui, D.S.; Chen, Y.; Tao, X.Y.; Xiang, W. Effect of prior cyclic loading on triaxial compression strength of sliding zone soil of the Huangtupo landslide. *Adv. Civ. Eng.* **2021**, *2021*, 9924995. [CrossRef]
6. Elger, J.; Berndt, C.; Rüpke, L.; Krastel, S.; Gross, F.; Geissler, W.H. Submarine slope failures due to pipe structure formation. *Nat. Commun.* **2018**, *9*, 715. [CrossRef] [PubMed]
7. Jamil, M.; Siddiqui, N.A.; Umar, M.; Usman, M.; Ahmed, N.; Rahman, A.H.; Zaidi, F.K. Facies analysis and distribution of Late Palaeogene deep-water massive sandstones in submarine-fan lobes, NW Borneo. *Geol. J.* **2022**, *57*, 4489–4507. [CrossRef]
8. Yin, M.; Rui, Y. Laboratory study on submarine debris flow. *Mar. Georesour. Geotechnol.* **2018**, *36*, 950–958. [CrossRef]
9. Zhang, W.C.; Randolph, M.F.; Puzrin, A.M.; Wang, D. Transition from shear band propagation to global slab failure in submarine landslides. *Can. Geotech. J.* **2019**, *56*, 554–569. [CrossRef]
10. Prior, D.B.; Suhayda, J.N.; Lu, N.Z.; Bornhold, B.D.; Keller, G.H.; Wiseman, W.J. Storm wave reactivation of a submarine landslide. *Nature* **1989**, *341*, 47–50. [CrossRef]
11. Quartau, R.; Ramalho, R.S.; Madeira, J.; Santos, R.; Rodrigues, A.; Roque, C. Gravitational, erosional and depositional processes on volcanic ocean islands: Insights from the submarine morphology of Madeira Archipelago. *Earth Planet. Sci. Lett.* **2018**, *482*, 288–299. [CrossRef]

12. Zhang, H.; Lu, Y.; Liu, X.; Li, X.; Wang, Z.; Ji, C. Morphology and origin of liquefaction-related sediment failures on the Yellow River subaqueous delta. *Mar. Petrol. Geol.* **2023**, *153*, 106262. [CrossRef]

13. Zen, K.K.; Yamazaki, H. Mechanism of wave-induced liquefaction and densification in seabed. *Soils Found.* **1990**, *30*, 90–104. [CrossRef] [PubMed]

14. Rahman, M.S. Wave-induced instability of seabed: Mechanism and conditions. *Mar. Georesour. Geotechnol.* **1991**, *10*, 277–299. [CrossRef]

15. Ulker, M.B.C.; Rahman, M.S.; Jeng, D.-S. Wave-induced response of seabed: Various formulations and their applicability. *Appl. Ocean Res.* **2009**, *31*, 12–24. [CrossRef]

16. Qi, W.; Li, C.; Jeng, D.; Gao, F.; Liang, Z. Combined wave-current induced excess pore-pressure in a sandy seabed: Flume observations and comparisons with theoretical models. *Coast. Eng.* **2019**, *147*, 89–98. [CrossRef]

17. Tong, L.; Zhang, J.; Zhao, J.; Zheng, J.; Guo, Y. Modelling study of wave damping over a sandy and a silty bed. *Coast. Eng.* **2020**, *61*, 103756. [CrossRef]

18. Ren, Y.P.; Xu, G.H.; Xu, X.B.; Zhao, T.L.; Wang, X.Z. The initial wave induced failure of silty seabed: Liquefaction or shear failure. *Ocean Eng.* **2020**, *200*, 106990. [CrossRef]

19. De Wit, P.J.; Kranenburg, C. The wave-induced liquefaction of cohesive sediment beds. *Estuar. Coast. Shelf Sci.* **1997**, *45*, 261–271. [CrossRef]

20. Zhang, H.; Liu, X.L.; Jia, Y.G.; Du, Q.Z.; Sun, Y.F.; Yin, P.; Shan, H.X. Rapid consolidation characteristics of Yellow River-derived sediment: Geotechnical characterization and its implications for the deltaic geomorphic evolution. *Eng. Geol.* **2020**, *270*, 105578. [CrossRef]

21. Dimitrova, R.S.; Yanful, E.K. Factors affecting the shear strength of mine tailings/clay mixtures with varying clay content and clay mineralogy. *Eng. Geol.* **2012**, *125*, 11–25. [CrossRef]

22. Wang, H.; Liu, H.J. Evaluation of storm wave-induced silty seabed instability and geo-hazards: A case study in the Yellow River delta. *Appl. Ocean Res.* **2016**, *58*, 135–145. [CrossRef]

23. Mathew, J.; Baba, M.; Kurian, N.P. Mudbanks of the southwest coast of India. I: Wave characteristics. *J. Coast. Res.* **1995**, *11*, 168–178.

24. Yu, H.Y.; Liu, X.L.; Lu, Y.; Li, W.J.; Gao, H.; Wu, R.Y.; Li, X.Y. Characteristics of the sediment gravity flow triggered by wave-induced liquefaction on a sloping silty seabed: An experimental investigation. *Front Earth Sci.* **2022**, *10*, 909605. [CrossRef]

25. Lamb, H. *Hydrodynamics*; Cambridge University Press: Cambridge, UK, 1932.

26. Sassa, S.; Sekiguchi, H.; Miyamoto, J. Analysis of progressive liquefaction as a moving-boundary problem. *Geotechnique* **2001**, *51*, 847–857. [CrossRef]

27. Eric, M.; Robert, A.D. Experimental observation of standing interfacial waves induced by surface waves in muddy water. *Phys. Fluids* **2011**, *23*, 096603. [CrossRef]

28. Guo, X.S.; Fan, N.; Zheng, D.F.; Fu, C.W.; Wu, H.; Zhang, Y.J.; Song, X.L.; Nian, T.K. Predicting impact forces on pipelines from deep-sea fluidized slides: A comprehensive review of key factors. *Int. J. Min. Sci. Technol.* **2024**, *34*, 211–225. [CrossRef]

29. Hsu, W.Y.; Hwung, H.H.; Yang, R.Y.; Liu, C.M. Interfacial wave motion caused by wave-mud interaction. *J. Vis.* **2012**, *15*, 215–224. [CrossRef]

30. Miyamoto, J.; Sassa, S.; Sekiguchi, H. Progressive solidification of a liquefied sand layer during continued wave loading. *Geotechnique* **2004**, *54*, 617–629. [CrossRef]

31. Ren, Y.P.; Xu, X.B.; Xu, G.H.; Liu, Z.Q. Measurement and calculation of particle trajectory of liquefied soil under wave action. *Appl. Ocean Res.* **2020**, *101*, 102202. [CrossRef]

32. Zen, K.K.; Jeng, D.S.; Hsu, J.R.C.; Ohyama, T. Wave-induced seabed instability: Difference between liquefaction and shear failure. *Soils Found.* **1998**, *38*, 37–47. [CrossRef]

33. Egan, G.; Cowherd, M.; Fringer, O.; Monismith, S. Observations of Near-Bed Shear Stress in a Shallow, Wave- and Current-Driven Flow. *J Geophys. Res. Oceans* **2019**, *124*, 6323–6344. [CrossRef]

34. Michallet, H.; Mory, M.; Piedra-Cueva, I. Wave-induced pore pressure measurements near a coastal structure. *J. Geophys. Res.* **2009**, *114*. [CrossRef]

35. Phillips, O.M. Wave interactions- the evolution of an idea. *J. Fluid Mech.* **1981**, *106*, 215. [CrossRef]

36. Jamali, M.; Lawrence, G. Viscous wave interaction due to motion of a surface wave over a sediment bed. *J. Offshore Mech. Arct. Eng.* **2006**, *128*, 276. [CrossRef]

37. Elgar, S.; Raubenheimer, B. Wave dissipation by muddy seafloors. *Geophys. Res. Lett.* **2008**, *35*. [CrossRef]

38. Wang, B.; Zen, K.; Chen, G.Q.; Zhang, Y.B.; Kasama, K. Excess pore pressure dissipation and solidification after liquefaction of saturated sand deposits. *Soil Dyn. Earthq. Eng.* **2013**, *49*, 157–164. [CrossRef]

39. Tzang, S.Y. Unfluidized soil responses of a silty seabed to monochromatic waves. *Coast. Eng.* **1998**, *35*, 283–301. [CrossRef]

40. Cui, L.; Jeng, D.S. Seabed liquefaction around breakwater heads at a river mouth: An integrated 3D model. *Ocean Eng.* **2021**, *242*, 110036. [CrossRef]

41. Aleebrahim, M.A.; Jamali, M. Experimental investigation of instability of fluid mud layer under surface wave motion. *Phys. Fluids* **2022**, *34*, 036602. [CrossRef]

42. Xu, G.H.; Liu, Z.Q.; Sun, Y.F.; Wang, X.; Lin, L.; Ren, Y.P. Experimental characterization of storm liquefaction deposits sequences. *Mar. Geol.* **2016**, *382*, 191–199. [CrossRef]
43. Yang, Z.N.; Zhu, Y.M.; Liu, T.; Sun, Z.Q.; Ling, X.Z.; Yang, J.M. Pumping effect of wave-induced pore pressure on the development of fluid mud layer. *Ocean Eng.* **2019**, *189*, 106391. [CrossRef]